Carbon Nanotubes as an Ultrafast Emitter with a Narrow Energy Spread at Optical Frequency

Chi Li, Xu Zhou, Feng Zhai, Zhenjun Li, Fengrui Yao, Ruixi Qiao, Ke Chen, Matthew Thomas Cole, Dapeng Yu, Zhipei Sun, Kaihui Liu,* and Qing Dai**

Ultrafast electron pulses, combined with laser-pump and electron-probe technologies, allow ultrafast dynamics to be characterized in materials. However, the pursuit of simultaneous ultimate spatial and temporal resolution of microscopy and spectroscopy is largely subdued by the low monochromaticity of the electron pulses and their poor phase synchronization to the optical excitation pulses. Field-driven photoemission from metal tips provides high light-phase synchronization, but suffers large electron energy spreads (3–100 eV) as driven by a long wavelength laser (>800 nm). Here, ultrafast electron emission from carbon nanotubes (≈1 nm radius) excited by a 410 nm femtosecond laser is realized in the field-driven regime. In addition, the emitted electrons have great monochromaticity with energy spread as low as 0.25 eV. This great performance benefits from the extraordinarily high field enhancement and great stability of carbon nanotubes, superior to metal tips. The new nanotube-based ultrafast electron source opens exciting prospects for extending current characterization to sub-femtosecond temporal resolution as well as sub-nanometer spatial resolution.

Ultrafast electron pulses, pumped by femtosecond lasers, allow the unprecedented study of various ultrafast phenomena with high spatial resolution,[1,2] such as subparticle ultrafast spectral imaging,[3] real-time protein–protein interactions,[4] and electromagnetic waveform microscopy.[5] Nevertheless, it remains challenging to simultaneously extend the spatial and temporal resolution of incumbent electron sources, which are mainly determined by the electron beam energy spread, which determines the beam spatial resolution, and high phase synchronization between the probe electron pulses and the pump light/electron pulses, which determines the temporal resolution.[6,7] It has proven difficult to date to simultaneously realize these two properties in incumbent electron source system, via both photon-driven (quantum) or field-driven (classical) approaches.[8]

Photon-driven photoemission sources are widely applied in state-of-the-art time-resolved electron microscopy and spectroscopy, as their highly monochromatic emission (≈0.7 eV of energy spread)[9] enables high spatial resolution (sub-nanometer) through photon energy—work function matching.[7] However, the temporal resolution (sub-picosecond) of different types of microscopy and spectroscopy is limited as the photon-driven emission is not well-synchronized to the optical phase.[1] Although great efforts have been devoted to improve the temporal resolution, through phase modulation in tailored near-field nanocavities following the photoemission process,[9,10] for example, the ultimate performance of the modulated electron beam still largely limited by the initial beam emission dynamics.

In contrast, field-driven photoemission typically occurs through subcycle durations, which naturally achieves electron pulses with high optical phase synchronization.[8,11] Indeed, this field-driven photoemission has been previously achieved from sharp metal tips under infrared excitation (wavelength >800 nm).[8,11–13] Unfortunately, the electron energy spread of such sources is extremely high (3–100 eV)[8,11,13] making them ill-suited for many emerging samples of interest. In this regime, the narrow electron energy spread strongly depends on the high field localization and short excitation wavelength.[8] Ultrasharp tips are essential to reduce the electron energy spread. Sharper tips give rise to higher field localization, and facilitate access to the field-driven photoemission regime at shorter wavelengths due to notably stronger field enhancement. However, this is difficult to achieve from traditional metal tips due to difficulties associated with their manufacturing coupled

Dr. C. Li, Dr. Z. J. Li, Dr. K. Chen, Dr. M. T. Cole, Prof. Q. Dai
Nanophotonics Research Division
CAS Center for Excellence in Nanoscience
National Center for Nanoscience and Technology
Beijing 100190, China
E-mail: daiq@nanoctr.cn
Dr. X. Zhou, Dr. F. R. Yao, Dr. R. X. Qiao, Prof. D. P. Yu, Prof. K. H. Liu
School of Physics
Academy for Advanced Interdisciplinary Studies
Collaborative Innovation Center of Quantum Matter
Peking University
Beijing 100871, China
E-mail: khliu@pku.edu.cn
Dr. F. Zhai
Department of Physics
Zhejiang Normal University
Jinhua 321004, China
Prof. Z. P. Sun
Department of Electronics and Nanoengineering
Aalto University
Tietotie 3, FI-02150 Espoo, Finland
E-mail: zhipei.sun@aalto.fi

to a need for a sufficiently robust material with a high damage threshold required to survive the high optical fields. The ultrasmall tip radius (≈1 nm), strong field enhancement and impressive structural stability (melting point >2000 K in vacuum), of carbon nanotubes (CNTs), have traditionally afforded highly coherent field electron emission capable of low energy spreads, small virtual source size, and high brightness.[14–19] As a static electron emission source, CNTs have been shown to outperform metal tips across almost all quantifiable metrics.[20]

In this work, for the first time, we demonstrate an ultrafast carbon nanotube-based, sub-nanometer electron source. The extremely sharp tips, coupled with their structural stability, allow extremely high optical-field localization, thereby enabling access to the field-driven photoemission regime at unprecedentedly short wavelengths as low as 410 nm, compared to 800–3000 nm as conventionally used for metallic tips.[8,12] As a result, a much narrower energy spread (≈0.25 eV) is obtained, an entire order of magnitude improved over previously demonstrated field-driven electron sources.[8,11] The photoemission process is schematically illustrated in **Figure 1**A. In our experiments, CNTs were grown by chemical vapor deposition (Supporting Information) and had a narrow normally distributed nominal tube radius between 0.5 and 1 nm (Figure 1B; Figure S2 of the Supporting Information).

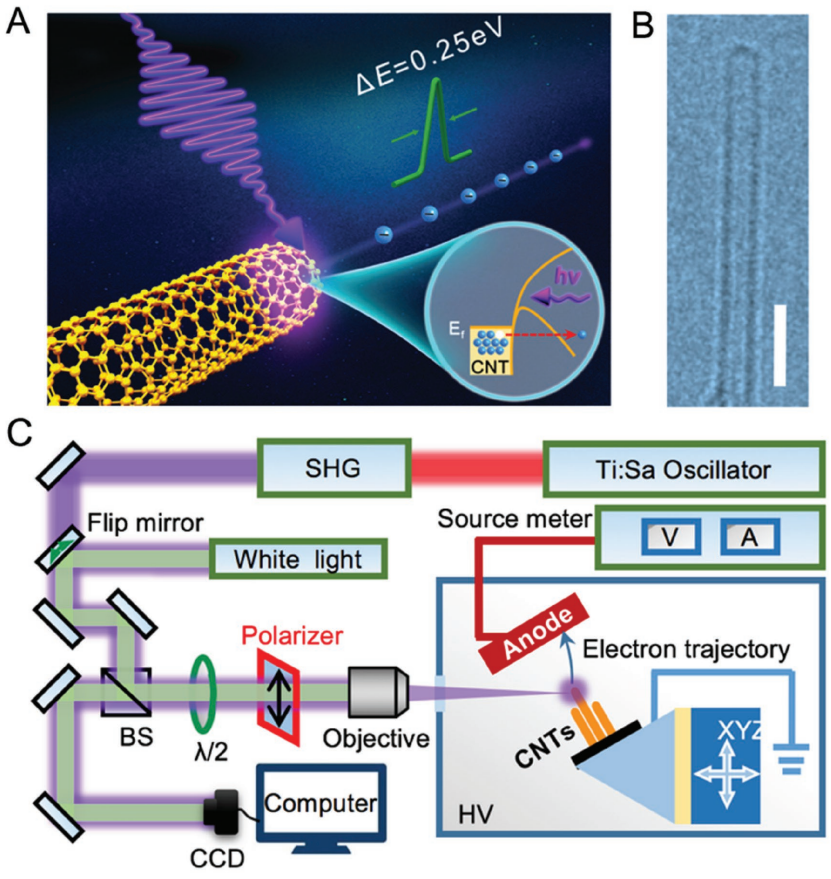

Figure 1. Highly coherent CNT-based photoemission source. A) Emission dynamics. B) High-resolution transmission electron microscopy image of a typical CNT under study. Scale bar: 5 nm. C) Experimental setup (SHG, second harmonic generation. CCD, charge-coupled device. BS, beam splitter. HV, high vacuum).

In the experiments, femtosecond pulses were focused onto the CNT tips under high vacuum, as illustrated in Figure 1C (see Experimental Section). Photoemission from the CNTs was found to depend strongly on the angle of linear polarization of the incident laser, as shown in **Figure 2**A. The polarization dependence exhibits a $\cos^6\theta$ behavior, where θ is the angle between the tip shank and the polarization of the input optical source. This suggested optically driven nonlinear photoemission as the observed translational symmetry only allows excitation by the field component vertical to the emitting surface.[21,22] This cosine curve also largely excludes any possibility of thermally induced field emission, which has been shown elsewhere to display a sinusoidal-like dependence on the polarization angle.[23]

Photoemission currents (I) were recorded as a function of incident laser power (P) under a bias voltage of 50 V, as shown in Figure 2B. The emission current at low pump power was approximately proportional to the fourth power of laser power, suggesting above threshold multiphoton photoemission.[24] The measured work function (ϕ) of the CNT (≈4.4 eV, see the Supporting Information for details) requires only two photons for photoemission. The enhanced emission nonlinearity indicates that electrons are sourced almost exclusively from the sharp CNT tips.[12] A downward deviation from the fourth power law to lower power law was found as the pump power increases, which presents transition from above threshold multiphoton photoemission to classical field-driven photoemission.[12,25,26] The approximate third power law (in the 3–5 mW region) of the I–P curve is also consistent with the $\cos^6\theta$ dependency of the polarization angle in Figure 2A, as the optical field adopts a square-law relation to the laser power. In the quasistatic field-driven regime, the photoemission current approximately follows the static field-emission model, which is given by cycle-average Fowler–Nordheim (FN) equation (fitting shown in Figure 2B):[27,28]

$$I = \frac{A(\beta F_0)^2}{\phi} \exp\left(\frac{-B\phi^{\frac{3}{2}}}{\beta F_0}\right) \quad (1)$$

where I is the emission current, $A = 1.56 \times 10^{-6}$ AV^{-2} eV, $B = 6.83 \times 10^9$ V eV$^{-3/2}$ V m^{-1}, β is a field enhancement factor, ϕ is the work function, and F_0 is incident laser field. The FN plot derived from the above current-field curve demonstrates a high degree of linearity, as shown in Figure 2C, which further confirms that the dominant emission has field-driven behavior. Thus, β can be calculated from the slope (S) of the linearized FN data, using the transformed form of Equation (1):

$$\ln\left(\frac{I}{F_0^2}\right) = \ln\left(\frac{A\beta^2}{\phi}\right) - \left(\frac{B\phi^{\frac{3}{2}}}{\beta}\right)\left(\frac{1}{F_0}\right) \quad (2)$$

and:

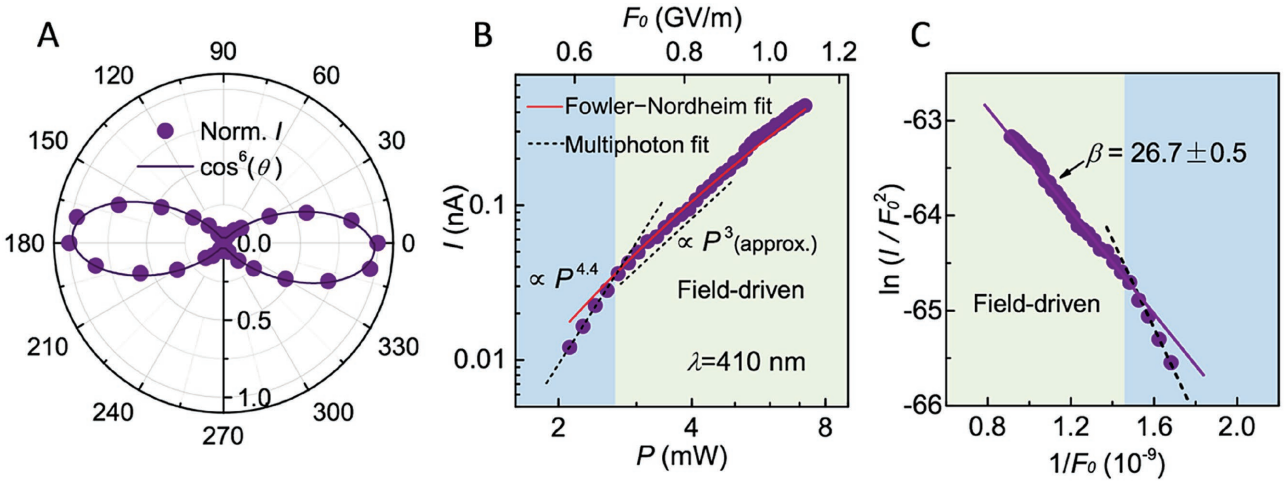

Figure 2. Field-driven photoemission at 410 nm pump wavelength. A) Normalized emission current (I) as a function of the angle of polarization (θ) of the input optical source. Note the emission currents show a $\cos^6(\theta)$ dependence. B) Emission current as a function of laser power (P) (bottom abscissa) and laser field (F_0) (top abscissa) at bias voltage (V_b) of 50 V. At low power range, multiphoton regime is noted, while field-driven regime is noted at higher power range. C) FN plot of the optically driven emission current, showing a field enhancement factor (β) of 26.7 ± 0.5. Green area in (B) and (C) corresponds to the field-driven regime region. λ, wavelength.

$$S = \frac{-B\phi^{\frac{3}{2}}}{\beta} \tag{3}$$

The calculated β was 26.7 ± 0.5 (approaching the value estimated from our finite element analysis, see the Supporting Information), which is approximately twice as large as those of conventional metal nanotips.[8,11,13] This explains why the visible field-driven wavelength operation is feasible with our CNT emitter, while near-infrared excitation is required for metallic tips.

The Keldysh parameter has been used to estimate the magnitude of the optical field required to support quasistatic electron tunneling, given by:[25]

$$\gamma = \omega\sqrt{2m\phi} \,/\, e\beta F_0 \tag{4}$$

where ω is optical frequency, ϕ is work function, m is the mass of the electron, and e is its charge, F_0 is the incident optical-field strength, and β is the field enhancement factor of the emitting tips. Recently, when strong field research was expanding into the realm of solid surfaces and nanostructures from its origin in gas molecules, it has been frequently observed that the transition to tunneling behavior occurs when $\gamma \approx 2$.[11,26] In this work, for a 3 mW 410 nm incident laser, the calculated γ was 1.83 ± 0.034, reasonably supporting the field-driven photoemission regime. With the same calculation method, γ is >2 (for example, $\gamma \approx 3.63$ at 2.3 mW), at above threshold multiphoton photoemission region (Figure 2C, dashed line). It is due to the much smaller β derived from the slope of the FN plot. This excludes the field-driven photoemission regime at this region (the pump power is less than 2.7 mW). Thus, both the cycle-averaged FN fitting and calculated the Keldysh γ, fully support that our CNT based ultrafast photoemission is operating in the field-driven tunneling regime at 3 mW 410 nm pump light. The field-driven photoemission regime is also supported by the electron energy distribution measurements as discussed below. We stress that this regime was previously unattainable at visible wavelengths due to the relatively low field enhancement and damage threshold of conventional metal tips. This finding provides an effective and convenient means of realizing narrow electron energy spreads.

Beam characterization was conducted using a retarding field method achieved by scanning the anode bias voltage (V_b) under varying laser powers (I–V measurements, **Figure 3**A). Three electron dynamics stages (marked as I, II, III in Figure 3A) were involved in the measurements. In stage I (the left-most region), all the emitted electrons exist in a fully retarding field (negative anode bias), such that no electrons can reach the anode as their kinetic energy cannot overcome the retarding potential. As the anode bias increases, the energetic electrons increasingly penetrate through the reduced retarding potential, and ultimately reach the anode (stage II, highlighted in pink in Figure 3A). In this regime, electrons with different kinetic energy require different collection potentials, such that the width of the potential range in this stage reflects the kinetic energy spread of the electrons, which behave increasing with the laser power increasing, in good agreement with theoretical descriptions reported elsewhere.[8] Due to the anisotropic local field around the tip alongside possible Coulomb repulsion, the emitted electrons diverge to form a cone beam,[12] which will be continuously focused and collected under the action of the increasing anode bias. This leads to a reduced rate of increase in the current, but still depends nonetheless on the laser power, as observed in stage III (the right most region). The slope increases with the laser power, indicating that high optical fields also broaden the electron emission angle. We note a constant current at the right region at an incident laser power of 3 mw suggesting that the generated electron beam has a very small emission angle.

In addition, the energy distribution data at 3 mW also support the field-driven photoemission regime. The kinetic energy of multiphoton photoemission electrons is typical equal to the

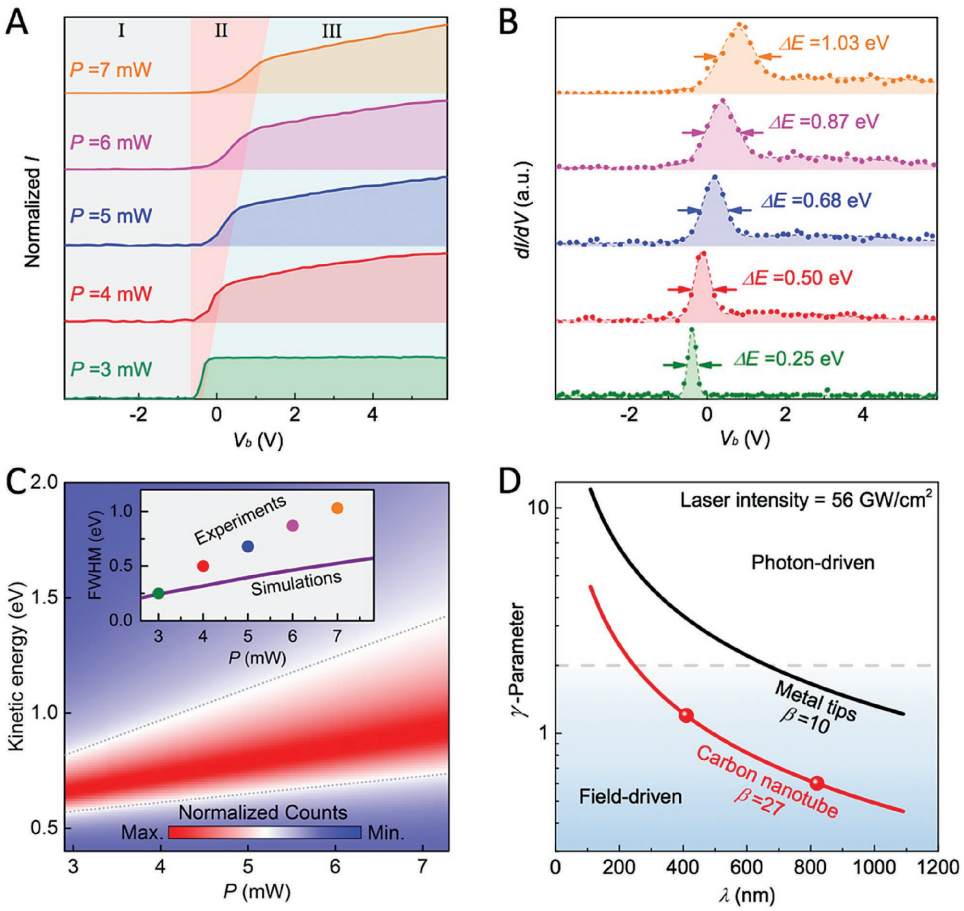

Figure 3. Electron beam characterization. A) Dependence of the normalized emission current on bias voltage (I–V_b) at different laser powers (P). Stage I: fully retarding region; stage II: fast collecting region; stage III: beam focusing region. B) corresponding dI/dV curves; the width of the peaks (FWHM) indicates the energy spreads (ΔE), while the shoulder indicates the beam divergence grade. C) Contour plot representation of the normalized counts as a function of P and kinetic energy, according to the extended Simpleman model. The FWHM is marked as the range between upper and lower dotted lines. The inset shows FWHM of the experimental ΔE (color dots) and simulated kinetic energy spectrum (purple line). D) Calculated Keldysh parameter γ as a function of wavelength at given β for carbon nanotube (≈27) and metal (≈10) and fixed laser intensity of 56 GW cm^{-2} (corresponding to 7 mW in present work). The two reds dots correspond to the results of this work.

difference between the photon energy and the material work function, for example, electrons generated from CNT ($\phi \approx 4.4$ eV) based two-photon (410 nm, 3 eV) photoemission is expected to have an average kinetic energy of ≈1.6 eV.[29] However, we did not obtain any current signal around −1.6 V bias voltage under 3 mW laser power (see Figure 3C). Our small kinetic energy (<0.5 eV) excludes the multiphoton photoemission dynamics, indicating that our CNT-based electron source is operating at the field-driven mode.

The energy distribution of the photogenerated electron beam can be determined directly from the differential spectrum of the above I–V_b curves,[29] as shown in Figure 3B. The peaks are derived from stage II, of which the width reflects the kinetic energy spread (ΔE) and demonstrates a clear dependency on the laser power. The right shoulders of the peaks are derived from stage III, of which the height reflects the beam divergence. As noted above, when the pump power was 3 mW, a very narrow energy spread down to 0.25 eV (full width at half maximum, FWHM, Gaussian fitting) was observed, which is more than one order of magnitude smaller than that of previously reported field-driven photoemission from metal tips (3–100 eV), and at least two times smaller than previously reported photon-driven sources.[9]

To elucidate this emission behavior, we compute the kinetic energy spectrum using experimentally derived parameters in an extended two-step Simpleman model.[8] The simulation includes a simplified FN tunneling model (first step—electron tunneling), and the interaction of the electrons with a strongly localized field near the tip (second step—electron propagation) (Supporting Information). Figure 3C shows the computed contour plot of individual kinetic energy spectrum as a function of laser power. The spectrum features are strongly modulated with the laser power: the FWHM (the range between the upper and lower dotted lines), refer to the electron energy spread and how this increases as a function of laser power, which is consistent with the experimental results observed in Figure 3B. At 3 mW (purple dashed line), our simulations reveal a kinetic energy spread of ≈0.24 eV, which is in good agreement with the experimental data (0.25 eV). The narrow energy spread and the small divergence of the electron pulses greatly benefit beam

line collimation and compression for functionally enhanced microscopy and spectroscopy. We note a broadening of the experimental energy spread relative to our simulations with increasing laser power (inset of Figure 3C). This may, in part, be attributed to enhanced tunneling probability near Fermi level energies when exposed to high optical fields,[30] as well as possible beam divergence attributed to the Coulomb repulsion,[31] both of which will contribute to the final measured energy spread (as illustrated in Figure S7, Supporting Information).

By calculating γ as a function of pump wavelength at a fixed surface intensity (56 GW cm^{-2}) for CNTs with $\beta = 27$ and metal tips with $\beta = 10$ (from refs. [8,11,13]), we realized that the higher capability of CNTs to access into field-driven photoemission under a much shorter pump wavelength than that of metal tips (Figure 3D). This suggests CNTs are an excellent platform for realizing broadband optical frequency-based electron emitters. In addition, electron pulses operating continuously for more than 50 h (see Figure S8, Supporting Information) at a high repetition rate of 80 MHz without obvious degradation, highlights the potential of the present CNT devices to operate as high brightness, long lifetime ultrafast electron sources.

Ultrafast processes, such as electronic transitions at the atomic scale, can evolve on time scales of a few femtoseconds and below. Advancing ultrafast imaging into this regime requires electron pulses of not only attosecond duration, but also high optical phase synchronization. Pulses generated from a traditional photon-driven photocathode cannot be shorter than the optical femtosecond pulses used for photoemission, and have a poor optical phase synchronization. In contrast, field-driven photocathodes provide a much shorter pulse duration due to the subcycle emission process, which lead to near ideal optical phase synchronization.

Here we have demonstrated field-driven photoemission from CNT emitters capable of generating extremely low energy spread (≈0.25 eV), which outperforms the current state-of-the-art field-driven electron sources by at least an order of magnitude. The high optical-field enhancement (≈27) in the engineered CNTs allows, for the first time, access to field-driven photoemission at unprecedently short wavelengths (410 nm)—an issue that continues to plague metallic sources—which potentially provides much improved beam coherence. Combining the unique geometrical and metrological properties of CNTs allows for simplified beam line collimation and compression system design in ultrafast microscopy and spectroscopy. The present findings suggest CNTs are a likely rich source for the realization of ultrafast electron guns, with the present findings going someway in contributing to sub-femtosecond electron microscopy and spectroscopy, therefore enabling new findings in ultrafast processes in materials with sub-nanometer resolution.

Experimental Section

Photoemission Experimental Setup: A schematic depiction of the experimental electron emission setup is shown in Figure 1C. Photoelectron emission from CNT arrays was triggered with 100 fs laser pulses, with a central wavelength of either 820 or 410 nm, at an 80 MHz repetition rate from a Ti: Sapphire ultrafast laser (Spectra-Physics, Mai Tai-Series, SHG). A standard Si photodiode power sensor (Thorlabs, Photodiode Power Sensor S120C) was used to measure the laser power. White light and a charge coupled device (CCD) were employed to monitor the sample position and the laser spot profile. The laser was linearly polarized with its polarization angle controlled via a polarizer and a half-wave plate. The laser was normally incident on the CNT tip via front illumination, which was focused to a 1.25/2.50 μm (FWHM, 410/820 nm) spot at the CNT cluster apex. Although the as-grown clusters contain many nanotubes, the growth kinetics were such that a few individual tubes protruded, repeatedly between growths, from these clusters producing a few isolated nanoscopic apex (Figure S5 of the Supporting Information), which is believed are the main photoemission sites giving the extremely high field enhancement there. These photocathode samples were mounted in a high-vacuum chamber (10^{-7} Torr). The anode was adjacent to the photocathode, some 400 μm distant, using a thick mica insulating spacer. The anode, together with the insulating separator, was placed directly on the surface of the photocathode with the CNT arrays centrally aligned. A Keithley 2400 source measurement unit was used to bias the anode with voltages of up to 50 V, with the anode current measured. Unless otherwise stated, the current measurements presented in the main text are those recorded at the anode. Every current data, collected by source meter, were acquired from an arithmetic average of 100 repeated measurements.

Supporting Information

Supporting Information is available from the Wiley Online Library or from the author.

Acknowledgements

C.L. and X.Z. contributed equally to this work. This work was supported by the National Basic Research Program of China (Grant Nos. 2016YFA0202000, 2015CB932400, and 2016YFA0300903), the National Natural Science Foundation of China (Grant Nos. 11427808, 51372045, 11474006, 5152220, and 91433102), the International Science and Technology Cooperation Project (No. 2014DFR10780, China), the Academy of Finland (Grant Nos. 276376, 284548, 295777, and 304666), TEKES (OPEC), Nokia foundation, the Oppenheimer Trust, and the European Union's Seventh Framework Programme (Grant No. 631610).

Conflict of Interest

The authors declare no conflict of interest.

Keywords

carbon nanotubes, electron sources, field-driven, monochromatic, ultrafast photoemission

Received: March 20, 2017
Revised: April 19, 2017
Published online: June 6, 2017

[1] A. H. Zewail, *Science* **2010**, *328*, 187.
[2] G. M. Vanacore, A. W. P. Fitzpatrick, A. H. Zewail, *Nano Today* **2016**, *11*, 228.
[3] A. Yurtsever, R. M. van der Veen, A. H. Zewail, *Science* **2012**, *335*, 59.
[4] H. N. Chapman, *Nature* **2011**, *470*, 73.
[5] A. Ryabov, P. Baum, *Science* **2016**, *353*, 374.

[6] P. Baum, *J. Phys. B: At., Mol. Opt. Phys.* **2014**, *47*, 124005.
[7] L. Kasmi, D. Kreier, M. Bradler, E. Riedle, P. Baum, *New J. Phys.* **2015**, *17*, 033008.
[8] G. Herink, D. R. Solli, M. Gulde, C. Ropers, *Nature* **2012**, *483*, 190.
[9] A. Feist, K. E. Echternkamp, J. Schauss, S. V. Yalunin, S. Schafer, C. Ropers, *Nature* **2015**, *521*, 200.
[10] C. Kealhofer, W. Schneider, D. Ehberger, A. Ryabov, F. Krausz, P. Baum, *Science* **2016**, *352*, 429.
[11] M. Kruger, M. Schenk, P. Hommelhoff, *Nature* **2011**, *475*, 78.
[12] R. Bormann, M. Gulde, A. Weismann, S. V. Yalunin, C. Ropers, *Phys. Rev. Lett.* **2010**, *105*, 147601.
[13] B. Piglosiewicz, S. Schmidt, D. J. Park, J. Vogelsang, P. Groß, C. Manzoni, P. Farinello, G. Cerullo, C. Lienau, *Nat. Photonics* **2013**, *8*, 37.
[14] W. A. Deheer, A. Chatelain, D. Ugarte, *Science* **2015**, *270*, 1179.
[15] N. de Jonge, Y. Lamy, K. Schoots, T. H. Oosterkamp, *Nature* **2002**, *420*, 393.
[16] H. Schmid, H. W. Fink, *Appl. Phys. Lett.* **1997**, *70*, 2679.
[17] A. G. Rinzler, J. H. Hafner, P. Nikolaev, L. Lou, S. G. Kim, D. Tomimek, P. Nordlander, D. T. Colbert, R. E. Smalley, *Science* **1995**, *269*, 1550.
[18] W. L. Yang, J. D. Fabbri, T. M. Willey, J. R. I. Lee, J. E. Dahl, R. M. K. Carlson, P. R. Schreiner, A. A. Fokin, B. A. Tkachenko, N. A. Fokina, W. Meevasana, N. Mannella, K. Tanaka, X. J. Zhou, T. van Buuren, M. A. Kelly, Z. Hussain, N. A. Melosh, Z. X. Shen, *Science* **2007**, *316*, 1460.
[19] J. Zhang, J. Tang, G. Yang, Q. Qiu, L. C. Qin, O. Zhou, *Adv. Mater.* **2004**, *16*, 1219.
[20] C. M. Collins, R. J. Parmee, W. I. Milne, M. T. Cole, *Adv. Sci.* **2016**, *3*, 1500318.
[21] P. Hommelhoff, Y. Sortais, A. Aghajani-Talesh, M. A. Kasevich, *Phys. Rev. Lett.* **2006**, *96*, 077401.
[22] D. Venus, M. J. G. Lee, *Phys. Rev. B* **1983**, *28*, 437.
[23] K. W. Hadley, P. J. Donders, M. J. G. Lee, *J. Appl. Phys.* **1985**, *57*, 2617.
[24] M. Kruger, M. Schenk, M. Forster, P. Hommelhoff, *J. Phys. B: At., Mol. Opt. Phys.* **2012**, *45*, 074006.
[25] L. V. Keldysh, *Sov. Phys. JETP* **1965**, *20*, 1307.
[26] R. G. Hobbs, Y. J. Yang, A. Fallahi, P. D. Keathley, E. D. Leo, F. X. Kärtner, W. S. Graves, K. K. Berggren, *ACS Nano* **2014**, *8*, 11474.
[27] R. G. Hobbs, Y. Yang, P. D. Keathley, M. E. Swanwick, L. F. Velásquez-García, F. X. Kärtner, W. S. Graves, K. K. Berggren, *Nanotechnology* **2014**, *25*, 465304.
[28] W. P. Putnam, R. G. Hobbs, P. D. Keathley, K. K. Berggren, F. X. Kärtner, *Nat. Phys.* **2017**, *13*, 335.
[29] H. Yanagisawa, M. Hengsberger, D. Leuenberger, M. Klöckner, C. Hafner, T. Greber, J. Osterwalder, *Phys. Rev. Lett.* **2011**, *107*, 087601.
[30] D. Lovall, M. Buss, E. Graugnard, R. P. Andres, R. Reifenberger, *Phys. Rev. B* **2000**, *61*, 5683.
[31] S. Hellmann, K. Rossnagel, M. Marczynski-Buhlow, L. Kipp, *Phys. Rev. B* **2009**, *79*, 035402.